Chem Soc Rev

This article was published as part of the

2008 Chemistry at Surfaces issue

Reviewing the latest developments in surface science

All authors contributed to this issue in honour of the 2007 Nobel Prize winner Professor Gerhard Ertl

Please take a look at the issue 10 table of contents to access the other reviews

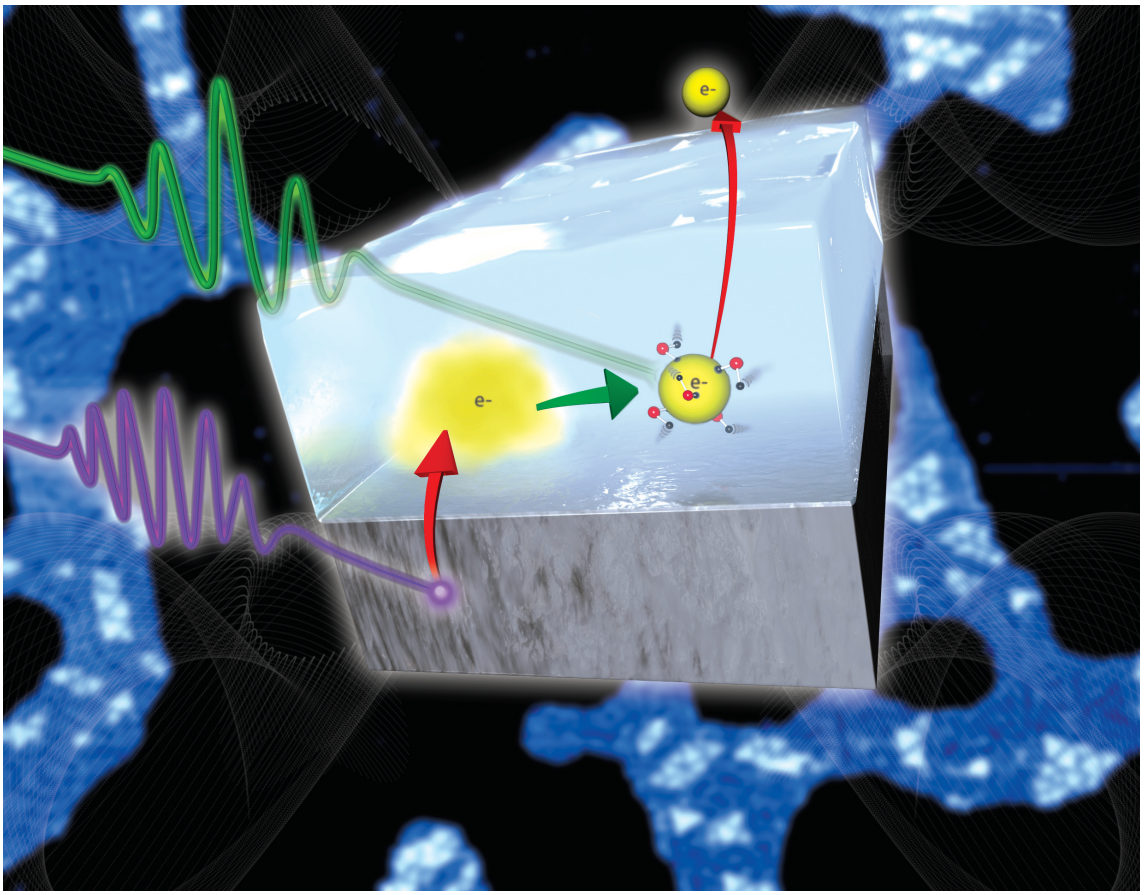

Scanning tunneling microscopy as a tool to study catalytically relevant model systems†

Ronnie T. Vang, Jeppe V. Lauritsen, Erik Lægsgaard and Flemming Besenbacher*

Received 2nd June 2008
First published as an Advance Article on the web 31st July 2008
DOI: 10.1039/b800307f

The surface science approach to catalysis, pioneered by 2007 Nobel Laureate in chemistry Gerhard Ertl, has helped revolutionize our understanding of heterogeneous catalysis at the atomic level. In this *tutorial review* we show how the scanning tunnelling microscope (STM), in combination with this surface science approach, is a very important tool for the study of catalytically relevant model systems. We illustrate how the high spatial and temporal resolution of the STM can be used to obtain quantitative information on elementary processes involved in surface catalyzed reactions. Furthermore, we show that the STM is an outstanding surface science tool to bridge the materials gap and the pressure gap between surface science experiments and real catalysis. Finally, we show that we are approaching an era where the atomic-scale insight gained from fundamental STM surface science studies can be used for the rational design of new catalysts from first principles.

Introduction

Spanning from large-scale production of basic chemicals to biological processes, catalysis constitutes a cornerstone of life as we know it. The list of additional technologies relying on catalysis is long and includes elimination of pollutants, production and distribution of sustainable energy, and production of pharmaceuticals. Despite the great importance and increasing application of catalysis in society, a detailed atomic-scale understanding of the principles governing the catalyzed chemical transformations involved in even simple reactions has in general not been established. This lack of understanding is mostly a consequence of the immensely complex structure of heterogeneous catalysts. An industrial high-surface-area catalyst is a material of high structural complexity consisting of nanoparticles dispersed on a high-surface-area support, and rather few experimental techniques are capable of providing structural insight into these complex nanostructures. The strategy normally followed is the one introduced by Gerhard Ertl and referred to as the "*Surface Science approach*": To simplify our considerations of reactions at surfaces, we study simple model systems consisting of either flat single-crystal surfaces or well-defined nanoclusters on surfaces under clean and well-controlled, often ultrahigh vacuum (UHV), conditions.[1]

Within the surface science approach a variety of different surface science techniques have been developed and employed since the early 1960s when UHV and modern science was established. However, one technique has revolutionized the surface science area, namely the scanning tunneling microscope

Interdisciplinary Nanoscience Center (iNANO) and Department of Physics and Astronomy, University of Aarhus, Aarhus, Denmark. E-mail: fbe@inano.dk; Fax: +45 8942 3690; Tel: +45 8942 3604

† Part of a thematic issue covering reactions at surfaces in honour of the 2007 Nobel Prize winner Professor Gerhard Ertl.

Erik Lægsgaard, Flemming Besenbacher, Jeppe V. Lauritsen and Ronnie T. Vang

Ronnie T. Vang is a postdoc in the Aarhus STM group. He obtained his PhD in 2005 from the University of Aarhus for his work on UHV and high-pressure STM studies of alloy and oxide model catalyst.

Jeppe V. Lauritsen is an assistant professor at the University of Aarhus working with UHV AFM. He obtained his PhD in 2003 for his work on STM studies of a hydrodesulfurization model catalyst.

Erik Lægsgaard is an associate professor at the University of Aarhus. He is co-founder of the Aarhus STM group and was the main person behind the development and construction of the Aarhus STM.

Flemming Besenbacher is a full professor and founding director of the Interdisciplinary Nanoscience Center (iNANO) at the University of Aarhus, and he is co-founder and head of the Aarhus STM group.

(STM), an outstanding tool capable of resolving the atomic-scale realm of surfaces, *i.e.* adsorbate structures and individual adsorbate signatures atom by atom and in certain cases even at high temporal resolution. Consequently, the STM has become an outstanding tool for monitoring the atomic and molecular dynamics, adsorbate-induced restructuring on surfaces, and chemical reactions on surfaces with relevance to heterogeneous catalysis.

In this tutorial review we illustrate, by a few examples, the use of STM for the study of fundamental surface processes relevant to heterogeneous catalysis. Our aim is to introduce this field to the reader and inspire further reading. It is not our intent to provide an in-depth and exhaustive review of the entire field, which can be found in already existing reviews or books, *e.g.* ref. 2.

Scanning tunneling microscopy

The fundamental principle of STM is conceptually rather simple. An atomically sharp metal tip is brought into such close proximity (3–5 Å) to a sample surface that an overlap occurs between the tip and the surface electronic wave functions, which decay exponentially in the junction gap. If a small bias voltage (V_t) is applied to the sample, electrons can tunnel elastically from filled tip states into sample tip states or *vice versa*, depending on the polarity of V_t. This vacuum tunneling, lending its name to the microscope, establishes a small tunnel current (I_t) within the nano-ampere range.

In the usual mode of operation, the STM tip is raster-scanned across the surface at a fixed bias voltage with a piezo-scanner used to control the x–y–z motion of the tip. Because the tunnel current depends strongly (exponentially) on the distance z between the tip and surface, the individual atoms on the surface will give rise to current variations as the tip is scanned across the corrugated surface; that is, the tunneling current will increase (or decrease) as the separation (z) between the tip and sample decreases (or increases). As the tip sweeps over surface structures, a feedback circuit regulates the tip–sample z separation in such a manner that the tunneling current is kept at the constant preset value I_0, and the z position of the tip, or rather the feedback signal, is recorded to produce a topographic map of the surface.

Despite the conceptual simplicity of the STM some precaution must be taken when interpreting STM images. Since the tip–sample separation is adjusted to produce a constant tunneling current, the resulting STM images represent *a priori* a rather complicated convolution of the surface geometric and electronic structure. Therefore, STM images cannot in general be interpreted as simply reflecting the surface topography, but rather represent images of the local density of states (LDOS) at the Fermi level projected to the tip apex position above the surface, as will be discussed below.

Catalysis studied by STM

The use of STM has become more and more widespread within the area of catalysis, and there are several good reasons for this. First of all, catalysis is an intrinsically local effect related to the active sites on the catalyst surface. These active sites are often step edges, kinks, atom vacancies or other defect sites, which can be extremely difficult to detect with the traditional averaging diffraction and scattering techniques. The STM with its ability to image single defects in real space and with atomic resolution is therefore ideally suited for studies of active sites on model catalyst surfaces. Furthermore, the image acquisition rate of state-of-the-art STMs has reached a level where dynamic surface processes can be visualized and analyzed in the form of so-called STM movies.[3] Finally, unlike most surface science tools the STM is not limited to operate under the extremely idealized ultra high vacuum (UHV) conditions, and it is thus possible to perform *in situ* STM studies at high pressures, whereby the conditions for most real catalysts are approached.[4] In the following a few examples from the literature will be used to demonstrate the use of STM in the studies of surface phenomena for model systems relevant to catalysis.

Imaging surfaces and single adsorbates

It is fair to say that STM has revolutionized or at least had an enormous impact on the area of surface science and catalysis over the past 20 years, simply due its capabilities to image individual atoms, molecules and defects. Much of the early work with STM was focused on semiconductor surfaces, which have a highly corrugated electronic structure due to dangling bonds and are therefore easily imaged with atomic resolution by STM.[5] Metal surfaces, on the other hand, typically have an electronic structure with low corrugation, which even led to speculations in the early days of the STM, that close-packed metal surfaces could not be atomically resolved with STM.[6] Since the first report on atomically resolved STM images of the Au(111) surface in 1987,[7] STM has matured tremendously to become a robust analytic tool that provides atomically resolved images on a routine basis.

The ability of the STM to image surface structures atom by atom makes it an important complementary technique to diffraction techniques that are best suited for large coherent surface structures. With the STM local structures such as point defects or domain boundaries can be characterized. Furthermore, the STM can be used to solve surface structures with very large unit cells and/or several equivalent domains or intermediate structures that are only found in coexistence with other surface structures. Such structures typically result in very complex diffraction patterns that are extremely difficult to resolve.

The STM technique is thus undoubtedly a unique tool, but there are cases where the extraction of certain types of information is less straight forward than desirable. Whereas STM images of pure and clean metal surfaces can be interpreted as simple topographic surface maps in most cases, it is often more complicated to interpret STM images of adsorbates. In the normally applied constant current mode, the STM images can be interpreted as contours of constant local density of states (LDOS) at the Fermi level of the sample surface at the position of the tip apex atom according to the *Tersoff–Hamann* theory.[8] On clean metal surfaces these contours are, to a first approximation, identical to the contours of total electronic charge density, and the STM images can therefore be interpreted as topographic maps of the surfaces.

For single individual adsorbates on metal surfaces the interpretation of STM images is sometimes somewhat

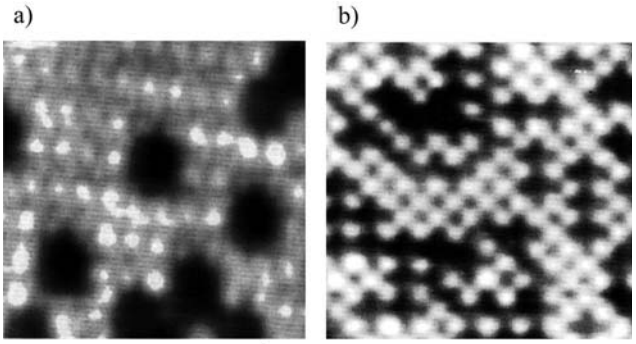

Fig. 1 STM images (30 × 30 Å^2) of O (a) and S (b) adsorbates on Ni(100). The O atoms are imaged as depressions in the (1×1) Ni lattice (bright spots), whereas the S atoms are imaged as bright protrusions.

counterintuitive. As shown originally by Lang,[9] adsorbates can be imaged as either depressions or protrusions depending on whether the adsorbate depletes or enhances the LDOS at the Fermi level, independent of the fact that the adsorbates geometrically reside in a position above the surface. This can be illustrated by imaging O and S adsorbates on Ni surfaces by STM (see Fig. 1). Oxygen adsorption on Ni(100) is known to result in $p(2\times2)$ and $c(2\times2)$ structures, corresponding to O coverages of $\frac{1}{4}$ and $\frac{1}{2}$ monolayer, respectively, with the O atoms adsorbed in fourfold hollow sites.[10] In STM images of O adsorbed on Ni(100) the O atoms appear as ~0.3 Å deep holes as seen in Fig. 1(a). On the other hand, sulfur atoms adsorb in a $c(2\times2)$ structure on Ni(100) and are imaged as ~0.3 Å high protrusions (Fig. 1(b)). The imaging of O and S atoms as holes and depressions, respectively, is not limited to the Ni(100) surface, but is rather a general trend in agreement with the model of Lang, which shows that O depletes and S enhances the LDOS at the Fermi level.[9]

Adsorbate–adsorbate interactions

Quantitative determination of adsorbate–adsorbate interactions is generally difficult to obtain because it requires information on the distribution of adsorbates for dilute coverages at which no long-range symmetry is present. But since it is possible to image individual adsorbates at various coverages with STM, adsorbate–adsorbate interactions can subsequently be determined. The typical way to extract quantitative information on the strength of adsorbate interactions and the interaction potentials is to compare the STM images with Monte Carlo simulations as demonstrated for example by the work of Österlund *et al.* for N adsorbed on Fe(100).[11] In Fig. 2(a) an atomically resolved STM image of a Fe(100) surface onto which N atoms have been adsorbed at a coverage of θ = 0.108 ML (monolayer) is shown: The N adsorbates are imaged as depressions as they cause a depletion of LDOS at the Fermi level in agreement with Lang's simple model,[9] and from the STM image it can be directly concluded that the N adsorbates are located in the high symmetry fourfold hollow site on Fe(100). Based on this and similar STM images Österlund *et al.* were able to determine the adsorbate distribution at different N coverages, from which the pair correlation

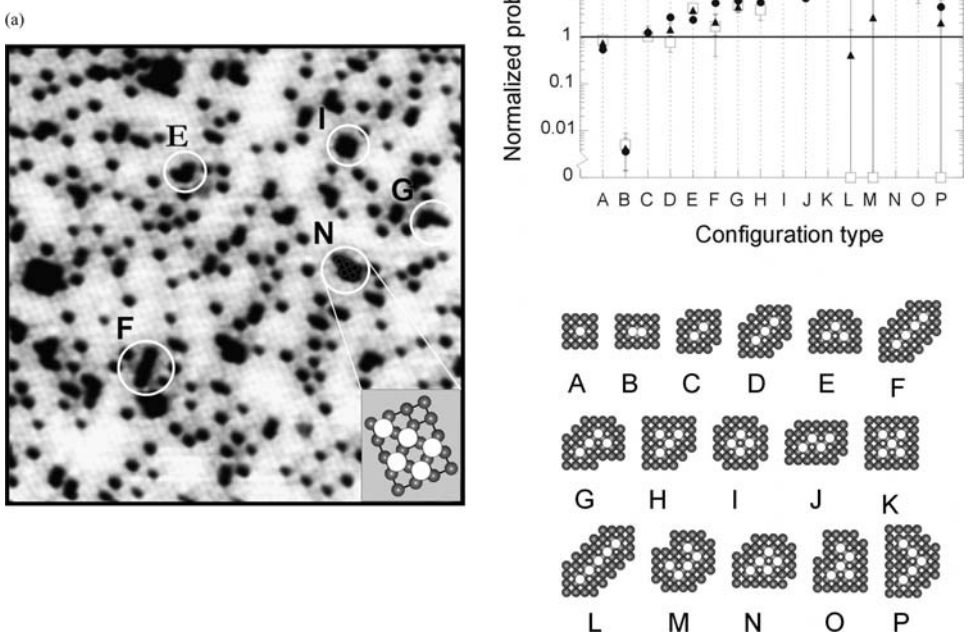

Fig. 2 (a) Atomically resolved STM image (160 × 154 Å^2) of N adsorbed on Fe(100) (θ = 0.108 ML). Some of the islands are labelled corresponding to the different island configurations used below. (b) Normalized probabilities for finding the different island configurations. The results of the Monte Carlo simulation are shown using both three-body (triangles) and pair (circles) interactions. Three-body interactions must be included to achieve a reasonable fit with the experimental results.

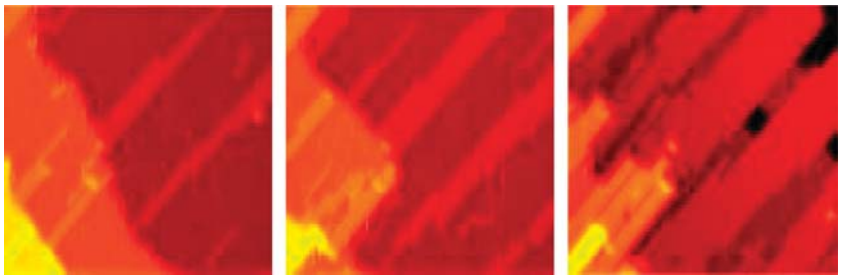

Fig. 3 Snapshots from an STM movie showing a Cu(110) surface during exposure to $\sim 10^{-8}$ Torr O_2 at room temperature. The removal of Cu atoms from step edges is accompanied by the nucleation of added rows in the [001] direction.

function, $g(j)$, for the N adsorbates could be determined. In the low coverage limit the pair correlation function is directly related to the pair potential, V, through $V_j = -kT\ln(g(j))$. Using this method the nearest and next nearest neighbour interaction potentials were determined to be 0.13 and −0.013 eV, respectively. The authors also went beyond this standard pair correlation analysis and performed Monte Carlo simulations, including many-body terms. The nearest and next nearest neighbour interactions (0.13 and −0.018 eV) found with this method were almost identical to the values obtained from the pair correlation method. However, it was shown that many-body terms are indeed very important in order to account for the exact adsorbate configuration (see Fig. 2(b)). The combination of STM and Monte Carlo simulations is one of several examples which demonstrate that STM experiments combined with theory yield important quantitative information on catalytic model systems.

Adsorbate-induced surface reconstruction

In the Langmuir formalism the surface of a catalyst is considered a static "checkerboard" of adsorption sites formed by a rigid, undistorted substrate lattice onto which gas phase molecules can adsorb, dissociate, react and form reactants which desorb without affecting the substrate template. However, in particular thorough STM studies have shown that this static view of the lattice represents a highly idealized picture which often is the exception rather than the rule for many adsorbates. Instead the surface has to be considered as a dynamic medium, the structure of which changes in response to a changing chemical environment induced by the adsorbates. Adsorbate-induced surface reconstructions can range from small relaxations of the lattice parameters to reconstructions mediated by long-range mass transport. By means of fast-scanning STM, the dynamic evolution of an adsorbate induced surface reconstruction can be followed at the atomic scale in real time, and in this way the mechanism of the formation of the reconstruction can be revealed directly, which is often a prerequisite for determining the resulting surface structure. This approach will be exemplified by the O-induced surface reconstruction of the Cu(110) surface.

It has been well known since the pioneering work of Ertl in 1967 that O_2 adsorbs dissociatively on the Cu(110) surface and induces a (2×1) reconstruction. Despite numerous experimental studies the exact structure of the (2×1) reconstruction was, however, not settled until 1990 when Ertl's group[12] and Jensen *et al.*[10] established the now widely accepted "added row" structure model. In the "added row" model adsorbed O atoms combine with Cu adatoms to form low-coordinated [001]-directed –Cu–O– added rows nucleating on top of the Cu(110) terrace. The nucleation and growth mode of this (2×1) reconstruction can be visualized in the form of STM movies, and in Fig. 3 a series of snapshots from such a movie is depicted. From the STM movie/images it is seen how the [001] directed added rows nucleate and grow from the step edges, *i.e.* Cu atoms detach from the step edges and diffuse on the surface until they combine with an adsorbed O atom and nucleate into –Cu–O–Cu added rows. The dynamics of the reconstruction is inherently linked to the final structure, and based on the unique insight provided by dynamic STM, the competing "buckled-row" structural model could be rejected because it does not involve long-range mass transport. Once completed, the "added row" structure is identical to a "missing row" structure, but in terms of mass transport these two models differ significantly. A "missing row" model would lead to the growth of the step edges due to Cu atoms squeezed out from the terrace as opposed to the "added row" model, where Cu is etched away and transported to the terrace. The STM data thus clearly identify the O-induced surface reconstruction of Cu(110) to be of the "added row" type. At higher oxygen coverages a $c(6\times2)$O reconstruction is formed with an oxygen coverage of 2/3 ML when completed. STM also played a crucial role in establishing the structure of this $c(6\times2)$ phase.[13] This example shows the close linkage between the dynamic surface mass-transport process and the final surface reconstruction, and it also stresses the fact that surfaces in the presence of strongly interacting adsorbates cannot, in general, be modelled as a static checkerboard. Instead models for adsorption and catalytic reactions must include the coupling to the substrate distortions as a prerequisite for understanding the trends of catalytic activities.

Surface diffusion

Surface diffusion of gas adsorbates is an integral part of surface catalyzed reactions proceeding according to the Langmuir–Hinshelwood mechanism. The determination of activation barriers for diffusion of relevant intermediate species is thus an essential part of any kinetic model of a catalytic reaction.

Diffusion of surface adsorbates has traditionally been analyzed by observing the time evolution of an initially localized surface concentration profile, which can be described by Fick's law.[14] In principle the diffusion constant, D, derived from such

an analysis, is related to the single jump events through the Einstein–Schmoluchowski relation $\langle(\Delta r)^2\rangle = 4Dt$, where $\langle(\Delta r)^2\rangle$ is the mean square displacement of a random walker after time, t.[14] In most practical cases this link between a macroscopic diffusion coefficient and single jump events is, however, very difficult to obtain due to, *e.g.*, the effect of finite coverage and the fact that no surface is completely uniform over extended macroscopic areas as those needed for typical measurements of concentration profiles.[14] To obtain reliable data for the activation barrier for diffusion events of single adsorbates it is therefore necessary to follow the motion of individual adsorbates, and the STM is indeed very well suited for this kind of study of surface diffusion.

In a very elegant set of measurements Ertl's group used time-lapsed STM to show that indeed the same diffusion barrier was derived from a (microscopic) profile analysis and from the analysis of the individual single jump events for N diffusion on Ru(0001).[15] By exposing the Ru(0001) surface to NO and observing that dissociation into adsorbed N and O takes place exclusively at the step edges, Zambelli *et al.* were able to prepare a very localized initial coverage of N adatoms at the step edges. The O atoms diffused rapidly on the timescale of the experiment, and the O atoms were clearly discernible from the N atoms, and so the temporal evolution of the N concentration profile could be monitored. In Fig. 4 the Ru(0001) surface is shown 6 min (a) and 2 h (b) after initial NO adsorption at room temperature, respectively, and it is clearly observed that the N atoms have diffused away from the step edge. From the analysis of the temporal broadening of the concentration profile, the diffusion constant could be determined. From temperature-dependent measurements the diffusion constant was found as a function of temperature, and from these data the activation energy for diffusion could be determined to be $E_a = 0.94$ eV. In another series of experiments the analysis of the diffusion of individual N atoms led to an almost identical diffusion constant.[15] The reason for the very good agreement is mainly due to the fact that the Fick analysis was in this case carried out with a relatively low initial N concentration and on a well-characterized area of the single-crystal surface. In this way the influence of adsorbate–adsorbate and adsorbate–defect interactions can be neglected.

In the study of surface diffusion, besides quantitative information on average diffusion constants, STM also offers unprecedented information about anisotropy, effects of local environment, *etc.*

Surface reactions

The observation of a surface-catalyzed reaction in real space and real time with atomic resolution is one of the obvious goals to pursue within the area of catalysis, and by means of dynamic STM studies this is indeed possible.[3] Ertl and co-workers studied the oxidation of CO on Pt(111) by performing titration experiments in which an O pre-covered Pt(111) surface was exposed to CO, and the reaction was monitored directly by *in situ* STM.[16] Fig. 5(a) shows an image of such an O pre-covered Pt(111) surface after exposure to 5×10^{-8} mbar CO for 140 sec at 247 K; at this point no reaction has taken place, and the O coverage is identical to the initial O coverage before CO exposure. The adsorbed CO has, however, led the adsorbed O to form large (2×2) islands due to the CO–O repulsion.[17] After 140 s the areas of the (2×2) O islands start to shrink, and simultaneously, islands with a $c(4\times2)$ structure, characteristic of CO on Pt(111), start to nucleate and grow on the Pt(111) surface (Fig. 5(b)). This reaction was interpreted as CO reacting with the pre-adsorbed O to form CO_2, which desorbs immediately, leaving behind vacancies for CO molecules to adsorb from the gas phase. It was thus possible to follow both reactants on the surface during the reaction, and it is clearly revealed that the reactants are not randomly distributed as assumed in the Langmuir–Hinshelwood model, but rather two different phases exist on the surface, and the reaction only occurs at the boundary between these two phases. This point was further quantified by obtaining the microscopic reaction rate from the sequence of STM images, and indeed this reaction rate was found to be proportional to the edge length along the phase boundary, rather than to the product of the two reactant surface coverages ($\theta_{CO}\cdot\theta_O$) as one would have expected from a simple Langmuir–Hinshelwood model. Based on STM experiments carried out at different temperatures, Wintterlin *et al.*[16] were also able to determine the activation energy for the reaction to

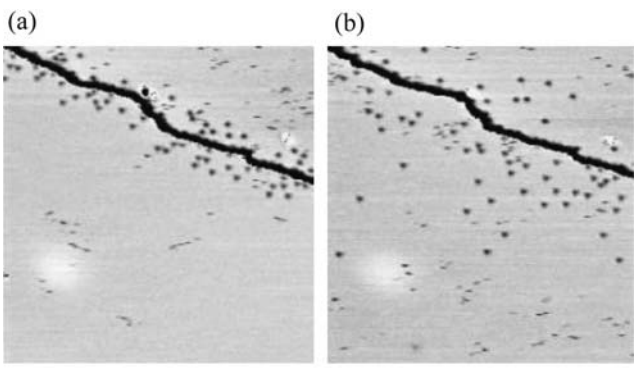

Fig. 4 (a) Ru(0001) surface 6 min after adsorption of 0.1 L NO. (b) The same area 2 h later. The large dark depressions are single N atoms, whereas the streaky dark features are O atoms, which diffuse on the same timescale as the line scanning rate. (Reprinted with permission from ref. 15. Copyright 1996, American Physical Society.)

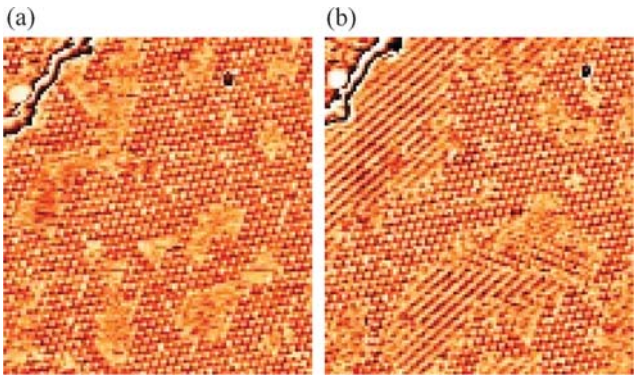

Fig. 5 O pre-covered Pt(111) surface during reaction with CO at 247 K imaged after (a) 140 s and (b) 600 s exposure to 5×10^{-8} mbar CO. The (2×2) O structure decreases, and the $c(4\times2)$ CO structure grows with time. (Reprinted with permission from ref. 16. Copyright 1997, AAAS)

be 0.49 eV, in excellent agreement with a previous molecular beam study which reported a value of 0.51 eV. The results of Wintterlin *et al.*[17] clearly demonstrate that a macroscopic quantity can be rationalized in terms of a microscopic understanding, thus revealing the true power of the STM in the study of model catalysts. These kinds of studies on single-crystal metals surfaces with pre-adsorbed oxygen have provided valuable insight into several catalytic oxidation processes. For some oxidation reactions, it is, however, important to perform the measurements in a gas mixture to simulate the catalytic reaction. This strategy is particularly favourable for reactions involving oxygen species different from those found when oxygen is pre-adsorbed on the surface. This approach is beautifully illustrated by the group of Madix and the group of Davies and Roberts in their studies of ammonia oxidation on Cu(110).[18,19] The use of variable-temperature STM is likewise extremely useful in the study of surface reactions, where it both serves to reduce or increase the reaction rate to fit with the image acquisition rate of the STM and to discriminate between different adsorbed species.

Bridging the gaps between surface science and catalysis with STM

The surface science approach introduced by Ertl has undoubtedly been extremely successful, and the study of model systems has contributed enormously to our understanding of heterogeneous catalysis. Within the surface science approach, however, gaps also exist between surface science and applied catalysis. These are usually referred to as the *materials gap* and the *pressure gap*. The materials gap refers to the structural gap between a single-crystal model surface and a real high-area catalyst consisting of highly dispersed nanoparticles on a porous support material. The pressure gap refers to the $\sim$13 orders of magnitude in pressure difference between the clean well-controlled UHV conditions inside a vacuum chamber and the high pressures existing inside a catalytic reactor under industrial conditions.

As opposed to many traditional standard surface science techniques, STM is a very versatile tool and in particular the STM is a truly local probe capable of operating at elevated pressures. These features make it possible to use the STM to bridge the different gaps by studying model systems consisting of nanoparticles grown on a planar support, and by performing the STM measurements at pressures ranging from UHV up to high pressures inside a dedicated high-pressure cell. The development of high-pressure STM was pioneered by Salmeron and Somorjai, who designed a dedicated HP-STM system and used a vacuum transfer cell for the sample transfer between the UHV chamber and the HP cell.[20] Later they improved their design so that they could perform an *in situ* transfer without loss of vacuum, and the upper temperature limit for the HP-STM studies was increased to 675 K.[21] Today several groups are working with high-pressure STM.[4]

The local probe nature of the STM makes it possible to study supported nanoclusters in great detail, and recently, this approach has been used to bridge the materials gap for, *e.g.*, metal/oxide systems. STM has revealed atomistic insight on real catalytic effects, such as the strong metal–support interactions for Pd deposits on TiO_2,[22] or the intriguing size-dependent catalytic oxidation by Au nanoparticles on TiO_2.[23]

Bridging the materials gap in hydrotreating catalysis

A very illustrative example of the unique potential of STM for providing new and valuable insight into the morphology and atomic-scale structure of supported model systems, very relevant to real catalysts, is the recent high-resolution STM studies of the important MoS_2-based hydrotreating catalyst. This catalyst is used world-wide in oil refineries for upgrading and purifying crude oil fractions by hydrogenation reactions (HYD) and removing sulfur (hydrodesulfurization, HDS) or nitrogen (hydrodenitrogenation, HDN). Besides the motivation that sulfur and nitrogen emission from fuels may be harmful to the environment, there is also the important technological aspect that even trace levels of sulfur left in fossil fuels lead to major complications in other processes treating the oil downstream. Sulfur is known to be a serious poison for other catalysts (*e.g.* Ni, Cu, Pd or Pt) which are used in other catalytic processes (hydrocracking, reforming, automotive catalysis, *etc.*). Currently, there is a huge and urgent demand for ultra-low-sulfur fuels and a better exploitation of heavy fuel reserves, and, consequently, better hydrodesulfurization processes and catalysts are needed. The most common catalyst, which separates sulfur embedded in organic compounds in the crude oil, consists of 2–3 nm wide single-layer MoS_2 nanoparticles mainly promoted with Co or Ni and supported on a porous alumina carrier.[24] For many years a considerable effort has been devoted to relate catalyst activity and selectivity to microscopic properties such as catalyst composition, geometric and electronic structure of the MoS_2 nanoclusters.[24] Only the edges of the S–Mo–S layers in MoS_2 are known to be catalytically active,[24] which means that the catalytic activity can only be studied on dispersed MoS_2 nanoclusters. This fact has rendered traditional surface science techniques based on plain single-crystal model catalysts rather ineffective, whereas studies on the real porous catalysts have been hampered by the resolution of the catalyst characterization techniques used and have thus not yielded the desired detailed structural insight needed to obtain a direct correlation between catalyst structure and its activity and selectivity. Consequently, a series of fundamental questions have remained unanswered due to the inability to provide exact direct space insight into the atomic structure of the dispersed MoS_2 nanoclusters. However, by means of STM it has recently become possible to successfully elucidate many aspects of the catalytic properties of the nanoclusters such as their detailed morphology and the active edge structures in MoS_2.[25] In particular, STM studies have revealed that the catalytic hydrodesulfurization (HDS) reactivity of the MoS_2 nanoclusters towards the most adverse sulfur containing hydrocarbons, the thiophenes, could be explained by an interplay between two different types of active sites present at the edge of single-layer MoS_2 slabs working in unison. The existence of different types of sites in MoS_2 catalysts had been proposed before based on macroscopic selectivity studies,[24] but the STM studies have provided the first atomic-scale view and revealed

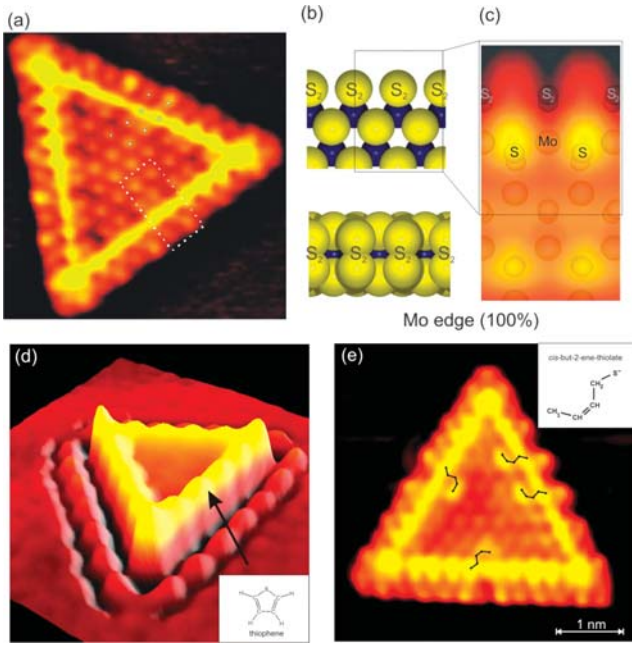

Fig. 6 (a) An atom-resolved STM image of a single-layer MoS_2 nanocluster. (b) The fully sulfided MoS_2 $(10\bar{1}0)$ Mo edge terminating the clusters. (c) STM simulation of the edge (d) 3D STM representation of thiophene adsorbed on the metallic brim (e) The MoS_2 nanocluster after exposure to atomic hydrogen and thiophene, revealing adsorbed *cis*-but-2-enethiolate ($C_4H_7S^-$) species.

the quite surprising nature of the active sites and their selectivity in HYD and HDS processes.

To achieve this detailed atomic-scale insight, a model system consisting of MoS_2 nanoclusters grown on a single-crystal gold substrate was synthesized.[26,27] The gold substrate was chosen since the so-called herringbone reconstruction[28] of the Au(111) gold facet forms the well-known herringbone reconstruction, which supports the synthesis of highly dispersed nanoclusters.[25,26] Furthermore, the noble character of the gold support was found to reduce substrate interactions so that primarily the intrinsic properties of single MoS_2 layers were studied. The atom-resolved STM image in Fig. 6(a) reveals the structure of a typical MoS_2 nanocluster synthesized on the Au substrate by sequential Mo deposition and sulfidation at 10^{-6} mbar H_2S pressure and 673 K. The nanocluster consists of a single S–Mo–S layer oriented with the (0001) facet in parallel with the substrate. Under sulfiding conditions, it was determined that the morphology of the MoS_2 nanocluster was always triangular independent of the cluster size. In the high-resolution STM image in Fig. 6, the protrusions on the cluster basal plane reflect the hexagonally arranged sulfur atoms in the topmost layer of MoS_2. The protrusions at the edges are, however, imaged out of registry with the S protrusions at the basal plane (see superimposed dots), and a characteristic and pronounced bright *brim* is observed to extend all the way around the cluster edge. It is important to emphasize that the STM measures electron tunneling to or from electronic states in the nanoclusters, and the STM images in general reflect a convolution of electronic and geometric features. In fact, both the bright brim and the apparent shifted registry of the edge protrusions visible in the STM images of the MoS_2 triangles in Fig. 6(a) can be traced back to a modified electronic structure at the edges, and further detailed analysis of the electronic structure has revealed the existence of two distinct one-dimensional electronic *edge states* on the fully sulfided Mo edges. Density functional theory (DFT) calculations have been used to investigate a large number of edge structures,[29] and only the so-called $(10\bar{1}0)$ Mo edges with a full coverage of S (forming S_2 dimers on the edge) were energetically stable and provided a match with the experiment in STM simulations (Fig. 6(c)). The electronic edge states for this edge are fully metallic in character, whereas bulk MoS_2 is a semiconductor with a band gap of 1.2 eV. The exact same Mo edge structure was recently also resolved with STM for multi-layer MoS_2 supported on graphite by Kibsgaard *et al.*, thus confirming that the findings for the MoS_2 nanoclusters are not dependent on the specific substrate support.[30]

From a simple coordination chemistry point-of-view, the fully sulfur-saturated Mo edges of the MoS_2 nanoclusters in Fig. 6(b) are normally not considered reactive, but due to the metallic character of the MoS_2 edges a chemistry that is rather different from the originally assumed one was found. Lauritsen *et al.* investigated the nature of the active sites on the cluster edges by selectively adsorbing thiophene (C_4H_4S) molecules in combination with hydrogen on the MoS_2 clusters.[31,32] After exposure of the fully sulfided nanocluster to thiophene alone at room temperature no adsorbed thiophene molecules were observed, but by reducing the temperature of the sample during exposure and imaging at 200 K it was observed how the metallic-like sites on top of the bright brim gradually became populated with thiophene molecules adsorbed with the aromatic-like ring system in parallel to the cluster plane (Fig. 6(d)). However, these thiophene molecules are only weakly physisorbed and desorb easily when the crystal is annealed. If, however the MoS_2 nanoclusters were first exposed to atomic hydrogen and then to thiophene at elevated temperature of 500 K, other, significantly more strongly adsorbed species were revealed at the position of the bright metallic brim, and the atom-resolved STM image in Fig. 6(e) shows several "bean-like" protrusions present in a position adjacent to the edges. From an interplay with DFT calculations these features were found to be thiophene-related reaction intermediates, *cis*-but-2-ene-thiolates ($C_4H_7S^-$), coordinated through the terminal sulfur atom to the metallic brim, resulting from a partial hydrogenation reaction occurring on the metallic brim states. The thiolates were calculated to be formed by a sequential hydrogenation of one of the double bonds in thiophene by hydrogen adsorbed on the edges (from the S–H groups) followed by C–S bond cleavage. The hydrogen driving this reaction originates from predissociated H atoms adsorbed on the terminal S atoms on the edges from S–H groups.[31] The combination of hydrogen atoms adsorbed on the edges in the form of S–H groups and the unusual sites for thiophene adsorption on the metallic brim presents a favorable situation for a hydrogenation reaction, and recent studies have indeed shown that the metallic sites are important for hydrogenation of both large S-containing molecules and N-substituted aromatic compounds.[33] Furthermore, STM experiments showed directly that the metallic sites are not

inhibited by H_2S adsorption, which explains the hydrogenation activity of the MoS_2-based catalyst even under highly sulfiding conditions.

The observed species in Fig. 6(e) resulting from the hydrogenation and C–S scission are associated with a simple thiol in which the S is known to be much easier to remove, and the final extrusion of this S may thus proceed on sulfur vacancies (so-called coordinatively unsaturated sites (CUS)), which have also been observed to form on the cluster edges with STM. In previous attempts to model the catalytic hydrogenation and hydrodesulfurization activity of MoS_2, typically only sulfur vacancies in various configurations were considered.[24] Very interestingly, and surprisingly, combined STM and DFT studies have revealed a new route for an initial activation of a relatively inert S-bearing molecule such as thiophene, and these processes are found to take place on the metallic brim states of the fully saturated Mo edges, which have the ability to accept or donate electrons and thus act as catalytic sites, just like ordinary reactive metal surfaces.

Upon the addition of cobalt or nickel to the MoS_2-based hydrotreating catalysts, the activity increases by more than an order of magnitude relative to that of the unpromoted MoS_2 and the selectivity in HYD, HDS and HDN reactions is also modified significantly.[24] Because only small amounts of Co and Ni are needed to induce these changes, the cobalt is characterized as a promoter rather than a catalyst in its own right. The enhanced activity has previously been shown to be correlated with the formation of bimetallic sulfided Co–Mo or Ni–Mo structures, termed Co–Mo–S–type structures.[24] The Co–Mo–S and Ni–Mo–S clusters do not have a unit cell in the crystallographic sense, but were proposed to exist as MoS_2 nanoclusters with molybdenum substituted by cobalt (or nickel) only at edge sites. The integration of Co or Ni into the MoS_2 matrix was predominantly considered to provide new types of active edge sites, but the exact location of such active sites and the origin of the promotion in activity and selectivity remained a puzzle for many years. By applying similar synthesis methods as for the unpromoted MoS_2 nanoclusters and co-depositing Co and Ni with Mo during sulfidation, Lauritsen *et al.* recently managed to synthesize model systems for the promoted CoMoS and NiMoS catalyst,[27,34] and for the first time they imaged the real-space structure of the promoted nanoclusters with STM. In accordance with the widely accepted Co–Mo–S model, a distinct tendency for Co and Ni to substitute Mo atoms at edge sites of single-layer MoS_2 nanoclusters was revealed, which leads to the truncation of the equilibrium cluster morphology relative to the strictly triangular morphology always observed for unpromoted MoS_2. The STM images of the nanoclusters are illustrated in the atom-resolved STM images in Fig. 7. The change in the equilibrium shape was driven by the favorable substitution of promoter atoms into the MoS_2 structure, and a detailed analysis of the atom-resolved STM images showed that the substitution occurred only at very specific edge sites in the Co–Mo–S and Ni–Mo–S nanoclusters. The truncated morphology of both Co–Mo–S and Ni–Mo–S nanoclusters implies that more than one fundamental type of low-indexed edge terminations of MoS_2 was present, *i.e.* both molybdenum edges and the sulfur edges terminate the cluster. In CoMoS

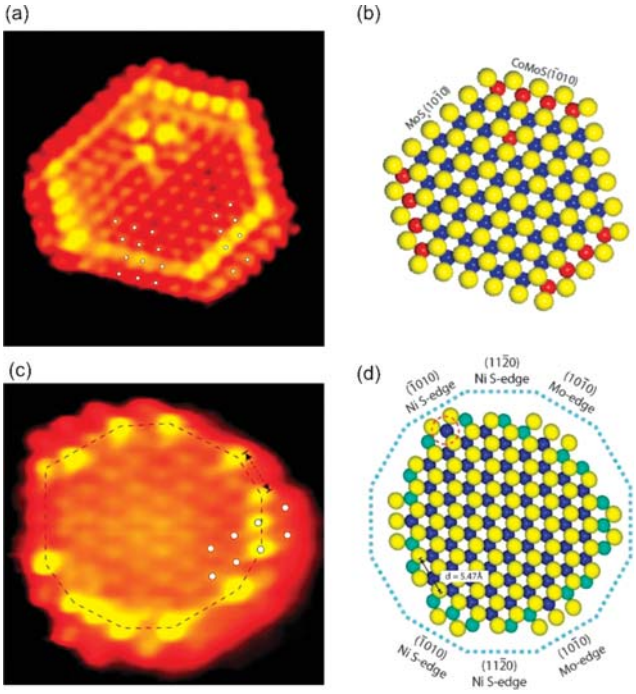

Fig. 7 (a) An atom-resolved STM image of a single-layer Co promoted MoS_2 nanocluster (Co–Mo–S). (b) Ball-model of a Co–Mo–S nanocluster (S: Yellow, Mo: Blue, Co: red). (c) An atom-resolved STM image of a single-layer Ni promoted MoS_2 nanocluster (Ni–Mo–S). (d) Ball model of a Ni–Mo–S nanocluster (S: yellow, Mo: blue, Ni: cyan).

(Fig. 7(a)), one edge type in the hexagonal truncated structure was found to be exactly identical to the $(10\bar{1}0)$ Mo edge observed for the unpromoted MoS_2 triangles, with the edge protrusions clearly imaged *out* of registry with the lattice of sulfur atoms on the basal plane and the bright brim along the edge. At the other edges Co had substituted Mo atoms on the $(\bar{1}010)$ S edge positions. On the basis of the STM images and the STM simulations based on DFT calculations, a tetrahedral coordination (Fig. 7(b)) of the cobalt atoms to S which agrees well with spectroscopic results reported for supported CoMoS catalysts, was revealed.[34]

For the Ni promoted clusters (Fig. 7(c)) the morphology of the clusters was even more complex since the affinity for Ni to replace Mo in the MoS_2 was not limited to just one type of edge. The Ni–Mo–S nanocluster shown in the atom-resolved STM image in Fig. 7(c) was observed to adopt the shape of a dodecagon, terminated by Mo edges, S edges and high-index $(11\bar{2}0)$ type edges, all of which contain Ni atoms. Again the structure and location and sulfur coordination of the Ni was analyzed in an interplay with DFT calculations, and a schematic model of the equilibrium Ni–Mo–S cluster (Fig. 7(d)) which agrees with the spectroscopic evidence from XAFS measurements was proposed.[34] Significantly, the promoted edges in both Co–MoS and Ni–Mo–S were observed in the STM images to exhibit very bright brim structures compared to the unpromoted edges, and a further band structure analysis based on DFT calculations revealed the existence of metallic one-dimensional edge states in both promoted clusters as well. This observation suggests that the metallic brim states

may not be limited only to unpromoted MoS_2, but may also exist in the promoted phase, where they could play a role for the different selectivities in HYD, HDS and HDN depending on the promoters. This is a subject that is currently being explored in STM studies of the Co–Mo–S and Ni–Mo–S nanoclusters using S- and N-containing probe molecules such as thiophene, dimethyl disulfide (CH_3–S–S–CH_3) and pyridine (C_5H_5N).

Bridging the pressure gap: high-pressure STM

A study by Longwitz *et al.* illustrates how high-pressure STM can be used to characterize the adsorption structure of CO on Pt(111) over the entire pressure range from 10^{-7} up to 760 Torr.[35] Adsorption structures at four different CO pressures at room temperature imaged by STM are shown in Fig. 8(a)–(d). At 10^{-7} Torr the well-known $c(4\times2)$ structure is observed, whereas Moiré superstructures are observed to form at higher CO pressures. These Moiré structures originate from the interference of a hexagonal CO overlayer, forming at high CO coverages ($> \frac{1}{2}$ ML) with the hexagonal Pt(111) surface layer. It is found that both the periodicity and the rotation of the CO Moiré structure change continuously with varying CO pressure. From the Moiré structure the coverage of CO could be deduced.[35] As depicted in Fig. 8(e), the CO coverage varies continuously as a function of the CO gas pressure, and furthermore the change in CO coverage is reversible, *i.e.* the adsorbed CO is in equilibrium with the gas phase CO.

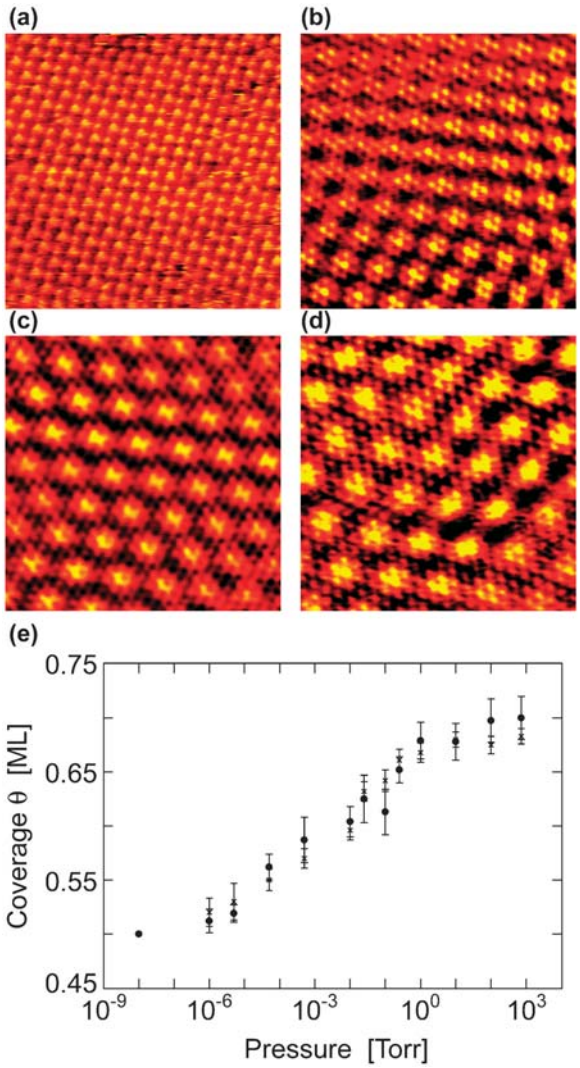

Fig. 8 (a–d) CO adsorption structures on Pt(111) at different CO pressures (Torr): (a) 10^{-7}, (b) 0.01, (c) 100 and (d) 720. The Moiré superstructure in (b)–(d) changes with the CO pressure. (e) CO coverage on Pt(111) as a function of the CO pressure.

The CO Moiré structures observed at high pressures also form at low temperature and low pressure as observed by both STM and by LEED.[35] Therefore, the CO/Pt(111) adsorption system can be said to exhibit no pressure gap. Similar conclusions are obtained from high-pressure studies of H/Cu(110), CO/Pt(110) and NO/Pd(111).[4] However, one example exists in the literature, NO on Rh(111), where Rider *et al.*, identified a novel (3×3) adsorption structure for NO pressures above 0.01 Torr,[36] and this (3×3) structure does not seem to form at low pressure and low temperature.

Even when similar adsorbate structures are formed at low pressure/low temperature and high pressure/high temperature, the high pressure data can provide valuable information about kinetic hindrance, entropy effects, surface dynamics and gas-phase equilibrium. High-pressure measurements are also important in identifying the active phase of the catalyst. The catalyst surface may undergo structural, morphological or even compositional changes in the presence of a high-pressure gas phase due to the strong adsorbate–substrate interaction. For bimetallic catalysts, high gas pressures may lead to surface segregation of one of the species owing to a strong interaction with the adsorbates.[37] Therefore, precautions must be taken when extrapolating UHV data on bimetallic catalysts to the situation of real operating catalysts, which might have a completely different surface composition as compared to surfaces studied under UHV conditions.

Vestergaard *et al.* indeed succeeded in imaging the CO-induced phase separation of a Au/Ni(111) surface alloy *in situ* and in real time by fast-scanning STM.[38] As discussed below, a Au/Ni alloy catalyst has been shown to be a more robust catalyst for the steam reforming of natural gas as compared to the standard Ni catalysts due to a reduced affinity for growing carbon whiskers, which can lead to a breakdown of the catalysts.[39] When prepared under UHV conditions, Au atoms substitute Ni atoms in the topmost layer of the Ni(111) surface to form a surface alloy in which the Au atoms are imaged as depressions by the STM, since they deplete the LDOS at the Fermi level (Fig. 9(a) and (b)). Following exposure to 1 bar of CO at room temperature, the morphology of the Au/Ni(111) surface alloy, however, changes dramatically as evidenced by STM (Fig. 9(c) and (d)). Small clusters are found to have nucleated homogeneously on the surface in response to the 1 bar CO exposure, and atomically resolved images reveal a clean Ni(111) substrate in between the nanoclusters. From a height analysis of the nanoclusters, it is confirmed that these clusters are single- and double-layer Au islands. This finding implies that upon CO exposure the Au/Ni(111) surface alloy phase separates into Au clusters on a pure Ni(111) substrate.

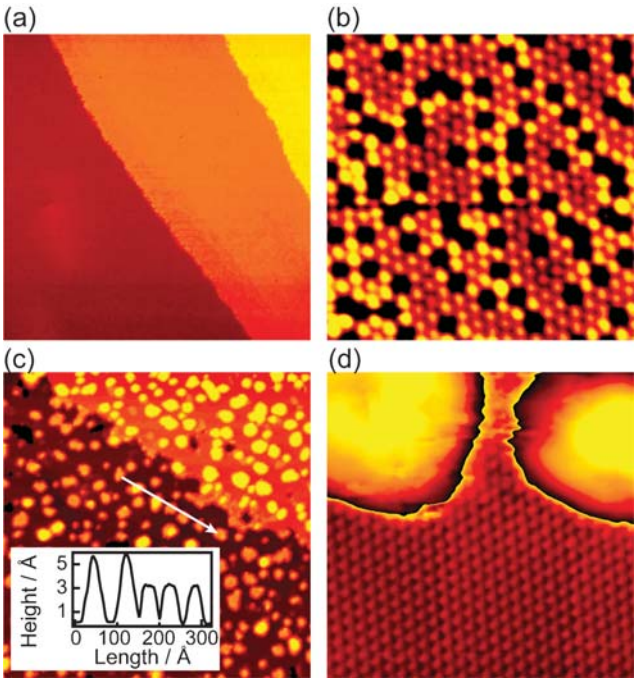

Fig. 9 (a) Au/Ni(111) surface alloy prepared by room temperature evaporation of Au onto Ni(111) followed by annealing at 800 K (800×800 Å^2). (b) Zoom-in on the same surface (50×50 Å^2). The Au atoms alloyed into the topmost layer of Ni(111) are imaged as depressions. (c) Au/Ni(111) after exposure to 1 bar CO at room temperature (800×800 Å^2). The height of the clusters as seen in the line scans can be identified as single- and double-layer Au islands. (d) A zoom-in (60×60 Å^2) shows the (1×1) Ni substrate in between the Au clusters.

The mechanism behind the phase separation of the Au/Ni(111) surface alloy was scrutinized by recording dynamic STM movies at intermediate CO pressures. In Fig. 10 snapshots from an STM movie recorded in a background of 13 mbar CO at room temperature are depicted. From this movie it is concluded that the Ni atoms in the topmost layer are removed from the step edges of the Au/Ni(111) surface due to the formation of volatile Ni-carbonyl species, leaving behind the Au adatoms, which nucleate into the Au nanoclusters. The formation of nickel carbonyl is a well-known process occurring on Ni surfaces exposed to high pressures of CO. Although this model system indicates that catalyst stability against high pressure exposure is an important issue, it is important to remember that these measurements only test the response of the Au/Ni(111) surface alloy to CO at room temperature, *i.e.* the measurements are not done at reaction conditions. For example under steam reforming reaction conditions the Au/Ni catalyst is likely to be stable, because carbonyl formation is suppressed at the high temperatures typically found inside steam reforming reactors.

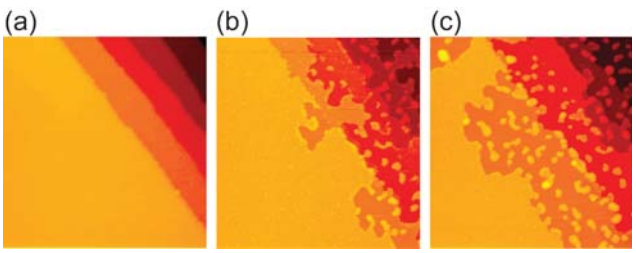

Fig. 10 STM images (1000×1000 Å^2) from a movie recorded in a background of 10 Torr CO at room temperature. The images show the surface after (a) 0 min, (b) 50 min, and (c) 75 min.

Further steps towards using STM to bridge the pressure gap in heterogeneous catalysis have been taken by Rasmussen *et al.*, who integrated an STM into a micro reactor volume,[40] and Hendriksen *et al.* used this "reactor STM" to surface morphological changes *in situ* during the oxidation of CO on a Pt(110) surface.[41] The *in situ* combination of STM and reactivity measurements has the potential of becoming a very powerful tool for the study of heterogeneous catalysts when further developed.

Designing catalysts from first principles

The surface science approach in general and the use of STM for the study of catalytically relevant model systems in particular have truly revolutionized our atomic level understanding of heterogeneous catalysis,[25,42,43] and the enormous importance of the surface science approach is clearly emphasized by the 2007 award of the Nobel prize to Gerhard Ertl. Today, we are on the brink of entering a new era in catalysis research in which the full step can been taken from atomistic surface science studies of model systems under well-controlled idealized conditions to the design of new high-surface-area industrial catalysts with improved properties.[25,43] This development is further accelerated by the recent advances in first principles theoretical modelling of elementary steps, and quantitative calculations of activation barriers using the density functional theory approach.[44,45] This rational approach to catalyst design will be illustrated by two examples in the following.

The first example is the novel Au/Ni alloy catalyst for the steam reforming reaction.[46] The steam reforming process, in which natural gas (mainly CH_4) reacts with steam (H_2O) to form synthesis gas (a mixture of H_2 and CO), is of major importance for, *e.g.*, oil refining (cracking, hydrotreating), fertilizer production (ammonia), or production of synthetic fuels by Fisher–Tropsch catalysis. Production of hydrogen by steam reforming is also predicted to play a key role in the implementation of a future hydrogen society. It is well known that Ni catalysts show high activity for the steam reforming reaction and are widely used in industrial plants. However, Ni also catalyzes the formation of graphite, which may lead to the growth of carbon filaments from the catalyst particles, and subsequently, an accelerated deactivation and eventually a complete breakdown of the catalyst.[39]

From an interplay of STM experiments and DFT calculations Besenbacher *et al.* showed that a Au/Ni alloy catalyst is more carbon resistant than the pure Ni catalyst, which results in a longer catalyst lifetime and thereby potentially reduces the need for expensive reactor shutdowns to replace a worn-out catalyst.[46] From STM studies it was shown that Au and Ni form a novel 2D surface alloy despite the fact that Au and Ni are immiscible in the bulk 3D phase. When Au is deposited on a Ni(111) surface, the Au atoms squeeze out Ni atoms and are substituted into Ni atom lattice positions in the surface layer,

and thereby a surface alloy is formed as illustrated by the atom-resolved STM image in Fig. 9(b).

The Au atoms are imaged as depressions in the STM image, which reflects the fact that the LDOS at the Fermi level at the positions of the Au atoms is lower than at the Ni sites.[46] Furthermore, in the STM images, those Ni atoms which have Au neighbours are imaged brighter than the Ni surface atoms which only have Ni neighbours, and this effect is even more pronounced for those Ni atoms with two Au neighbours. It was concluded that the electronic structure was significantly perturbed for the Ni atoms with neighbouring Au atoms, and DFT calculations confirmed that this effect cannot be explained by an outwards relaxation of the Ni atoms. The Au/Ni(111) thus basically contains three types of Ni atoms: Ni atoms with no Au nearest neighbours (nn), Ni atoms with one Au nn, and Ni atoms with 2 Au nn. The DFT calculations further revealed that the tendency of the surface to bind carbon and form graphite is strongly impeded by the presence of the Au atoms substituted into the topmost layer of the Ni(111) surface. The Ni atoms with Au nearest neighbours have a higher barrier for activation of hydrocarbon molecules, such as CH_4, and the overall effect of the Au atoms is thus to increase the selectivity at the expense of a slightly reduced activity.

These fundamental findings inspired the synthesis of a high-surface-area, $MgAl_2O_4$-supported Ni catalyst (with 16.5 wt% Ni), which was modified with 0.3 wt% Au.[46] By means of extended X-ray absorption fine structure spectroscopy (EXAFS), it was verified that the Au is indeed alloyed into the first layer of the Ni catalyst. This high-surface-area Au–Ni catalyst was then tested by measuring the activity of steam reforming of *n*-butane, and comparing this to a similar measurement on a pure Ni catalyst (see Fig. 11). *n*-Butane was used to test the activity because it is known to give rise to the most severe graphite formation problems. Whereas the conventional Ni catalyst is deactivated fairly rapid due to the formation of graphite filaments, as confirmed by, *e.g.* electron microscopy, it was found that the conversion factor for the new Au–Ni catalyst is almost constant. This finding implies that for this new catalyst, the graphite formation is significantly reduced. These results show that the new high-surface-area Au–Ni alloy catalyst for the steam reforming process is superior to the conventional Ni catalysts because it is more resistant to the formation of carbon filaments. This research illustrates that we are approaching a point where

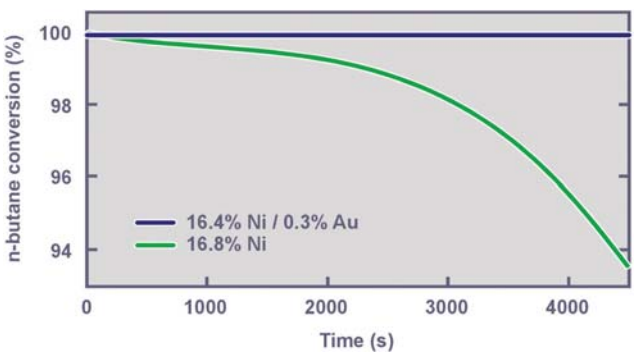

Fig. 11 Conversion of *n*-butane as a function of time for a Au/Ni alloy catalyst and a pure Ni catalyst.

fundamental insight into surface structure and reactivity can be applied directly to the design of new catalysts.

Another example of rational catalyst design is the work of Vang *et al.* on ethylene dissociation on Ni(111).[47] The reactivity of catalytic surfaces is often dominated by very reactive low-coordinated atoms, such as step-edge sites.[48] However, very little knowledge exists about the influence of such step edges on the selectivity in reactions of larger molecules involving multiple reaction pathways. Such detailed information could be very valuable in the rational design of new catalysts with improved selectivity. In general, the *selectivity* of a given catalytic reaction is as or even more important than the *activity*. From an interplay between STM experiments and DFT calculations Vang *et al.* showed that the activation of ethylene (C_2H_4) on Ni(111) follows the trend of higher reactivity for decomposition at step edges as compared with the higher-coordinated terrace sites. It was shown that the step-edge effect is considerably more pronounced for the C–C bond breaking than for the C–H bond breaking, and thus steps play an important role in the bond-breaking selectivity. Furthermore, the authors demonstrated how the number of reactive step sites can be controlled by blocking the steps with a brim of Ag atoms along the step edges.

This approach to nanoscale design of catalysts was subsequently exploited in the synthesis of a new high-surface-area AgNi alloy catalyst, which was tested in hydrogenolysis experiments.[47] When ethylene was exposed to Ni(111) at room temperature, a brim of decomposed ethylene was formed along the upper step edges (see Fig. 12(a)). The coverage of this brim of decomposed ethylene did not increase by exposure to larger amounts of ethylene, which shows that the reaction is self-poisoning. It was thus concluded that only the step edges are active sites for the decomposition of ethylene on Ni(111) at room temperature.

To gain information on the different reaction pathways in the decomposition of ethylene on Ni(111), the STM data were complemented by DFT calculations on both the flat Ni(111) surface and the stepped Ni(211) surface. The activation barriers were calculated for the two possible initial steps: dissociation (C–C bond-breaking) and dehydrogenation (C–H bond-breaking). The calculations showed that both energy barriers (dehydrogenation and dissociation) on the stepped surface were significantly lower than the lowest barrier (dehydrogenation) on the flat surface, consistent with the high reactivity of the step sites observed in the STM study. The DFT calculations furthermore showed that the two barriers are similar on Ni(211), whereas dehydrogenation is favoured by *ca.* 0.5 eV over dissociation on Ni(111). This finding implies that the selectivity of the Ni(111) surface towards ethylene dissociation or dehydrogenation, is determined to a large extent by the presence of free step edge sites. The DFT results thus show that the selectivity towards dehydrogenation would increase if the step edges were not active. To test this observation, Vang *et al.* successfully blocked the edge sites by depositing Ag on the Ni(111) surface. After annealing at elevated temperatures it was demonstrated by STM that Ag wetted all Ni(111) step edges as a thin brim of Ag atoms (see Fig. 12(b)), and it was subsequently shown that the Ag indeed lowered the reactivity of the step edges because ethylene did not decompose on the Ag-decorated step edges.

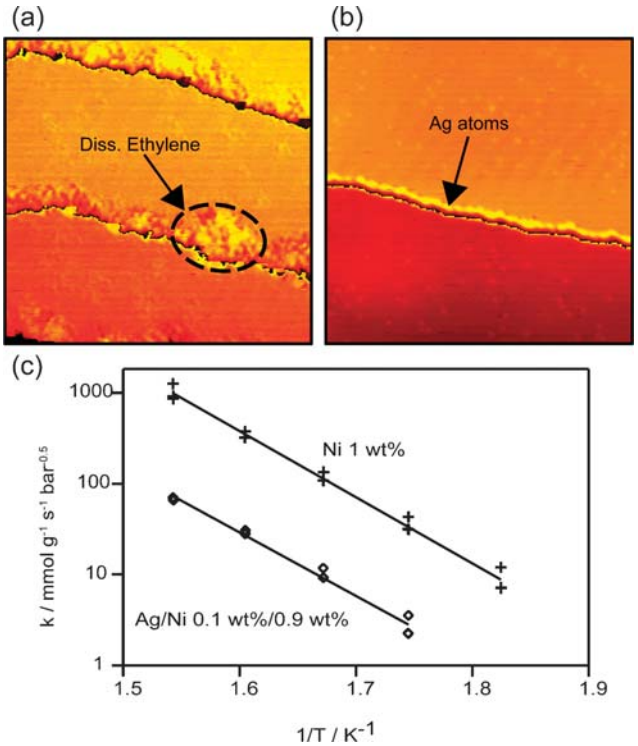

Fig. 12 (a) STM image (200 × 200 Å^2) of a Ni(111) surface after exposure to I L ethylene at room temperature. Reaction products have nucleated along the upper step edges. (b) STM image (400 × 400 Å^2) of a Ni(111) surface with the step edges covered with a row of Ag (bright protruding line along the step edge). (c) Arrhenius plots of the rate constant for ethane hydrogenolysis over $Ni/MgAl_2O_4$ and $Ag/Ni/MgAl_2O_4$.

Based on these fundamental STM and DFT studies, an oxide-supported high-surface-area AgNi catalyst was synthesized and compared to a pure Ni catalyst for the hydrogenolysis of ethane ($C_2H_6 + H_2 \rightarrow 2CH_4$), which is the simplest possible reaction to probe the activity for C–C bond breaking. The results are depicted in Fig. 12(c), and it is seen that the rate constant for ethane hydrogenolysis is indeed reduced by approximately an order of magnitude by the addition of Ag to the Ni catalyst. The rate does not drop to zero because not all step edges are covered with Ag on the highly dispersed oxide-supported catalyst.

Again it is demonstrated how fundamental surface science (STM and DFT) results have formed the base of the nanoscale design of new high-surface-area catalysts, which allows us to control the bond-breaking selectivity of the Ni catalysts between dissociation and primary dehydrogenation. This bond-breaking selectivity will eventually show up in the selectivity between the final products in, *e.g.*, hydrogenolysis or dehydrogenation of hydrocarbons.

Conclusions

Over the past three decades the STM has matured from a complicated home-built instrument present in only a few labs to a very versatile and powerful technique used for surface science studies. The enormous success of the STM is owing to its unique and unparalleled high spatial and temporal resolution enabling imaging of single atoms and molecules on surfaces and their motion in real time. An area where the STM has had great impact is the study of model systems for heterogeneous catalysts following the surface science approach introduced by Gerhard Ertl. Catalysis is very often related to special active sites such as steps, kinks, defects or vacancies, which makes the STM the technique of choice for the study of surface catalyzed reactions at the atomic scale. With the atomic-scale insight gained we are now approaching a new era in which *trial and error* methods for the development of new catalysts are replaced by *catalyst design from first principles*, where the fundamental atomic-scale knowledge allows us to propose and design new catalysts. STM and its sister scanning probe technique, atomic force microscopy, have a promising future for the study of catalytically relevant model systems.

References

1 G. Ertl and H.-J. Freund, *Phys. Today*, 1999, 32–38.
2 P. R. Davies and M. W. Roberts, *Atom Resolved Surface Reactions: Nanocatalysis*, RSC Publishing, Cambridge, UK, 2007.
3 F. Besenbacher, E. Lægsgaard and I. Stensgaard, *Mater. Today*, 2005, **8**, 26–30.
4 R. T. Vang, E. Lægsgaard and F. Besenbacher, *Phys. Chem. Chem. Phys.*, 2007, **9**, 3460–3469.
5 R. M. Feenstra, in *Scanning Tunneling Microscopy and Related Methods*, ed. R. J. Behm, N. Garcia and H. Rohrer, Klüwer Academic Publishers, Dordrecht, 1990, vol. 184, p. 211.
6 R. J. Behm, in *Scanning Tunneling Microscopy and Related Methods*, eds. R. J. Behm, N. Garcia and H. Rohrer, Klüwer Academic Publishers, Dordrecht, 1990, vol. 184, p. 173.
7 V. M. Hallmark, S. Chiang, J. F. Rabolt, J. D. Swalen and R. J. Wilson, *Phys. Rev. Lett.*, 1987, **59**, 2879–2882.
8 J. Tersoff and D. R. Hamann, *Phys. Rev. Lett.*, 1983, **50**, 1998–2001.
9 N. D. Lang, *Phys. Rev. Lett.*, 1985, **55**, 230–233.
10 F. Jensen, I. Stensgaard, F. Besenbacher and C. Klink, *Vacuum*, 1990, **41**, 337–339.
11 L. Österlund, M. Ø. Pedersen, I. Stensgaard, E. Læsgaard and F. Besenbacher, *Phys. Rev. Lett.*, 1999, **83**, 4812–4815.
12 T. Gritsch, D. Coulman, R. J. Behm and G. Ertl, *Phys. Rev. Lett.*, 1989, **63**, 1086–1089.
13 F. Besenbacher, *Rep. Prog. Phys.*, 1996, **59**, 1737–1802.
14 R. Gomer, *Rep. Prog. Phys.*, 1990, **53**, 917–1002.
15 T. Zambelli, J. Trost, J. Wintterlin and G. Ertl, *Phys. Rev. Lett.*, 1996, **76**, 795.
16 J. Wintterlin, S. Völkening, T. V. W. Janssens, T. Zambelli and G. Ertl, *Science*, 1997, **278**, 1931–1934.
17 C. T. Campbell, G. Ertl, H. Kuipers and J. Segner, *J. Chem. Phys.*, 1980, **73**, 5862–5873.
18 A. F. Carley, P. R. Davies and M. W. Roberts, *Chem. Commun.*, 1998, 1793–1794.
19 X. C. Guo and R. J. Madix, *Faraday Discuss.*, 1996, 139–149.
20 B. J. McIntyre, M. Salmeron and G. A. Somorjai, *J. Vac. Sci. Technol., A*, 1993, **11**, 1964–1968.
21 J. A. Jensen, K. B. Rider, Y. Chen, M. Salmeron and G. A. Somorjai, *J. Vac. Sci. Technol., B*, 1999, **17**, 1080–1084.
22 R. A. Bennett, C. L. Pang, N. Perkins, R. D. Smith, P. Morrall, R. I. Kvon and M. Bowker, *J. Phys. Chem. B*, 2002, **106**, 4688–4696.
23 M. Valden, X. Lai and D. W. Goodman, *Science*, 1998, **281**, 1647–1650.
24 H. Topsøe, B. S. Clausen and F. E. Massoth, *Hydrotreating Catalysis*, Springer Verlag, Berlin–Heidelberg, 1996.
25 J. V. Lauritsen and F. Besenbacher, *Adv. Catal.*, 2006, **50**, 97–147.
26 S. Helveg, J. V. Lauritsen, E. Lægsgaard, I. Stensgaard, J. K. Nørskov, B. S. Clausen, H. Topsøe and F. Besenbacher, *Phys. Rev. Lett.*, 2000, **84**, 951–954.
27 J. V. Lauritsen, S. Helveg, E. Lægsgaard, I. Stensgaard, B. S. Clausen, H. Topsøe and F. Besenbacher, *J. Catal.*, 2001, **197**, 1–5.

28 J. V. Barth, H. Brune, G. Ertl and R. Behm, *Phys. Rev. B: Condens. Matter Mater. Phys.*, 1990, **42**, 9307–9317.
29 M. V. Bollinger, J. V. Lauritsen, K. W. Jacobsen, J. K. Nørskov, S. Helveg and F. Besenbacher, *Phys. Rev. Lett.*, 2001, **87**, 196803.
30 J. Kibsgaard, J. V. Lauritsen, K. Morgenstern, E. Lægsgaard and F. Besenbacher, in preparation.
31 J. V. Lauritsen, M. Nyberg, J. K. Nørskov, B. S. Clausen, H. Topsøe, E. Lægsgaard and F. Besenbacher, *J. Catal.*, 2004, **224**, 94–106.
32 J. V. Lauritsen, M. Nyberg, R. T. Vang, M. V. Bollinger, B. S. Clausen, H. Topsøe, K. W. Jacobsen, F. Besenbacher, E. Lægsgaard, J. K. Nørskov and F. Besenbacher, *Nanotechnology*, 2003, **14**, 385–389.
33 P. G. Moses, B. Hinnemann, H. Topsøe and J. K. Nørskov, *J. Catal.*, 2007, **248**, 188–203.
34 J. V. Lauritsen, R. T. Vang and F. Besenbacher, in *Applied Scanning Probe Methods VII*, eds. B. Bushan and H. Fuchs, Springer-Verlag, Berlin–Heidelberg, 2007, pp. 197–224.
35 S. R. Longwitz, J. Schnadt, E. K. Vestergaard, R. T. Vang, E. Lægsgaard, I. Stensgaard, H. Brune and F. Besenbacher, *J. Phys. Chem. B*, 2004, **108**, 14497–14502.
36 K. B. Rider, K. S. Hwang, M. Salmeron and G. A. Somorjai, *Phys. Rev. Lett.*, 2001, **86**, 4330–4333.
37 E. Christoffersen, P. Stoltze and J. K. Nørskov, *Surf. Sci.*, 2002, **505**, 200–214.
38 E. K. Vestergaard, R. T. Vang, J. Knudsen, T. M. Pedersen, T. An, E. Lægsgaard, I. Stensgaard, B. Hammer and F. Besenbacher, *Phys. Rev. Lett.*, 2005, **95**, 126191.
39 J. R. Rostrup-Nielsen, J. Sehested and J. K. Nørskov, *Adv. Catal.*, 2002, **47**, 65–139.
40 P. B. Rasmussen, B. L. M. Hendriksen, H. Zeijlemaker, H. G. Ficke and J. W. M. Frenken, *Rev. Sci. Instrum.*, 1998, **69**, 3879–3884.
41 B. L. M. Hendriksen and J. W. M. Frenken, *Phys. Rev. Lett.*, 2002, **89**, 046101.
42 J. Wintterlin, *Adv. Catal.*, 2000, **45**, 131–206.
43 J. V. Lauritsen, R. T. Vang and F. Besenbacher, *Catal. Today*, 2006, **111**, 34–43.
44 K. Honkala, A. Hellman, I. N. Remediakis, A. Logadottir, A. Carlsson, S. Dahl, C. H. Christensen and J. K. Nørskov, *Science*, 2005, **307**, 555–558.
45 K. Reuter, D. Frenkel and M. Scheffler, *Phys.Rev. Lett.*, 2004, **93**, 116105.
46 F. Besenbacher, I. Chorkendorff, B. S. Clausen, B. Hammer, A. M. Molenbroek, J. K. Nørskov and I. Stensgaard, *Science*, 1998, **279**, 1913–1914.
47 R. T. Vang, K. Honkala, S. Dahl, E. K. Vestergaard, J. Schnadt, E. Lægsgaard, B. S. Clausen, J. K. Nørskov and F. Besenbacher, *Nat. Mater.*, 2005, **4**, 160–163.
48 T. Zambelli, J. Wintterlin, J. Trost and G. Ertl, *Science*, 1996, **273**, 1688–1690.